

# HARMONIC METHOD FOR SIMULATING UNSTEADY MULTISPOOL INTERACTIONS

**Feng Wang\***

Oxford Thermo-Fluids Institute  
Department of Engineering Science  
University Of Oxford  
UK

**Luca di Mare**

Oxford Thermo-Fluids Institute  
Department of Engineering Science  
University Of Oxford  
UK

## ABSTRACT

*Modern civil jet engines arrange components on spools with different rotational speeds in order to improve compressor stall margin, overall engine performance, etc. The unsteady interactions among these components can be significant and should be considered at an early design stage if possible. URANS is a common approach to simulate these unsteady effects, but the disparity in time scales in a multispool simulation can lead to expensive URANS simulations. Harmonic methods are effective and efficient approaches to simulate unsteady interactions among turbomachinery components, but their applications to multispool simulations remain a challenge. The objective of this paper is to address this challenge. This paper extends the Favre-averaged non-linear harmonic method to simulate multispool turbomachinery components using a unified bladerow interface which transfer disturbances through bladerows with arbitrary blade counts at any rotational speed. The regularization of non-reflective boundary condition is described for certain circumferential wave number of the zero-frequency mode. The capability of the proposed approach is demonstrated by simulating the transfer of hot streaks through full 3D high- and intermediate-pressure turbines in a three-shaft engine. The temperature distributions from the harmonic method show good agreement with direct unsteady simulation in terms of the mean flow and the instantaneous flow. The radial migration of the hot streaks towards the hub are captured very well by the proposed harmonic method. The required wall-clock time of the harmonic method is roughly 240 times smaller than the whole annulus URANS simulation. This demonstrates the proposed method can be an efficient design tool to trace hot streaks in multispool turbines at the early design stage.*

---

\*Corresponding author, email: feng.wang@eng.ox.ac.uk

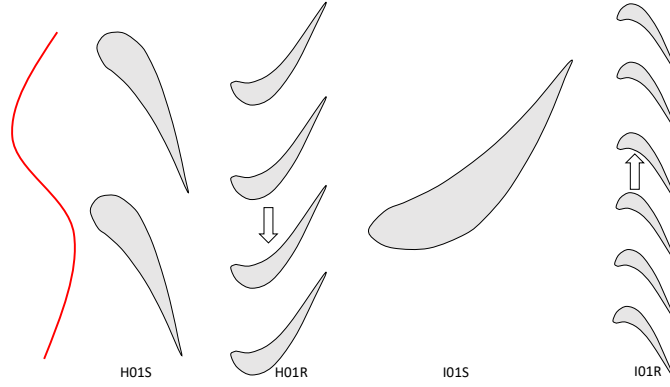


**FIGURE 1.** Schematic of HP and IP turbines on the blade-to-blade plane with inlet disturbance.

## Introduction

The interactions of turbomachinery components which are arranged on different spools are unsteady in nature and not negligible. In modern architectures with reduced axial gaps between components, interactions across multiple spools can be detrimental to engine performance and mechanical integrity. Steady Reynolds-Averaged Navier-Stokes (RANS) simulation with mixing plane is currently the workhorse in turbomachinery design but this approach is unable to capture such unsteady interactions. A direct unsteady simulation, i.e. Unsteady RANS (URANS), can be used but the computational cost will increase by two or three orders of magnitude compared to steady simulations. Furthermore, since the components can have different rotational speeds, URANS simulation are more expensive than the unsteady simulations where all the components are on the same shaft.

Figure 1 illustrates the transmission of a low EO disturbance (e.g. hot streak) at the NGV (H01S) inlet through the High Pressure (HP) and Intermediate Pressure (IP) turbines. In a multispool setting, the rotational speeds  $\Omega_{H01R}$  and  $\Omega_{I01R}$  are different and their values are not rational multiples of one the other. If stochastic perturbations which are related to flow turbulence are modelled by a suitable turbulence model, assume there is no vortex shedding (or its impact is of secondary importance to the transmission of the low EO disturbance) or stalls, the frequencies of which are difficult to known apriori, three deterministic or periodic time scales are present and they are related to  $\frac{2\pi}{\Omega_{H01R}}$ ,  $\frac{2\pi}{\Omega_{I01R}}$  and  $\frac{2\pi}{|\Omega_{I01R} - \Omega_{H01R}|}$ . The duration of the direct unsteady simulation needs to be based on the longest among them but the choice of numerical time step needs to be chosen based on the shortest among them to retain temporal numerical accuracy. Moreover, since  $\Omega_{H01R}$  is not a multiple of  $\Omega_{I01R}$  or vice versa, there is no clear definition of one periodicity in the bladerows and, accordingly, a time-mean flow.

To efficiently compute the unsteady interactions, one can make the URANS faster without changing the underlying numerical algorithms by optimizing a CFD code (i.e. vectorization) and leveraging many-core CPU architectures and GPU. The other approach is to develop a computationally efficient algorithm. These algorithms can lead to a reduction of computational cost by several orders of magnitude. A judicious usage of these approaches can strike a good balance between modelling fidelity and computational efficiency. Furthermore, the computationally efficient algorithms can always benefit from code optimization and many-core CPU architectures and

GPU, this can lead to a further reduction of the computational cost.

Harmonic methods are computationally efficient approaches for periodic unsteady flows and they assume that unsteady flows are deterministic and frequencies of interest are known a-priori. A time-domain periodic problem can be cast as a steady problem in the frequency domain, therefore flow periodicity can be achieved considerably faster than in time-domain methods. Furthermore, for computations involving multiple bladerows, harmonic methods generally only require one passage for each bladerow in the computation. These advantages allow harmonic methods to be an effective tool to approximate unsteady multispool interactions at the design stage.

Time-linearized methods were successfully applied to unsteady bladerow interactions for inviscid [1], viscous [2] and multistage [3] interactions. These linearized method ignored the coupling among the harmonics and the mean flow and became less accurate as flow perturbations becomes larger. One popular approach to include these non-linear coupling is the Harmonic Balance method [4]. This approach solved a finite set of steady-state solutions at fixed time-levels in the time domain simultaneously, and all these time-level solutions are coupled through periodic boundaries and a spectral source term. An alternative approach is the Non-Linear Harmonic (NLH) [5] or Favre-averaged NLH (FNLH) [6] method. The latter is more rigorous and easier to implement, since it does not require the explicit conversion between conservative and primitive variables in the time-mean flow. HB inherently can deal with strong non-linear flows and NLH/FNLH needs to include high order terms in the linearized flow to take into account the non-linear coupling of the harmonics [7–9]. The main difference between HB and FNLH is that HB can be implemented as a time-domain method while FNLH requires a dedicated linearized NS solver to compute the Fourier modes. However FNLH tends to be a more flexible approach and can be effectively used as a multi-fidelity tool. Coupling among the harmonics and mean flow can be switched off easily if the unsteady flow is approximately linear. Furthermore, FNLH can also been extend to compute flow disturbances arising from geometry non-uniformity [10, 11]

For multistage simulations with multiple fundamental frequencies, which is a challenging topic for harmonic methods, HB can group harmonics into different sets [12]. This can be considered as a linearization of the HB method. The cross-coupling between the sets are ignored but they are indirectly coupled through the mean flow in a fashion similar to FNLH. Extending NLH/FNLH to multistage simulations is more straightforward compared to HB and applications can be found in simulating compressor clocking [13], tracing hot stream migrations in multistage turbines [14] or whole engine simulations [15].

There is very limited research on extending harmonic methods to multispool simulations, which has significant industry relevance. For instance, having a credible prediction of the temperature traverse in the HP and IP turbines is of great importance to turbine aero-thermal design and the current design approach which uses steady mixing plane is unable to predict such temperature traverse.

The contribution of this paper is to extend the FNLH method to approximate unsteady multispool interactions, in particular, tracing hot streak migrations in HP and IP turbines. To the authors' best knowledge, there is no previous careful study on applying harmonic methods to trace hot streaks in full 3D multispool turbines. Spatial and temporal modes of the hot streaks in HP and IP turbines will be derived. Regularization of non-reflective treatment for zero-frequency mode will be highlighted. This work will demonstrate that FNLH

can be a cost-effective tool to predict the temperature traverse in multispool turbines compared to URANS.

This paper is organized as the following: the FNLH method is briefly outlined in the first place, the non-reflective treatment and regularization for zero-frequency mode are then described. After that, the spatial and temporal modes of the hot streaks across the multispool turbine is derived. Two case studies are then presented to demonstrate the performance of the proposed harmonic method to transmit a disturbance in 4 ducts with multiple rotational speeds and trace hot streak migrations in an industrial two-stage multispool turbine. This is followed by the conclusions of the paper.

## Favre-averaged Non-Linear Harmonic Method

FNLH approximates periodic unsteady interactions in a multirow machine with arbitrary blade counts efficiently based on the assumption that frequencies of interest are known a-priori. The mean flow is represented as Favre-averaged [16] primitive variables and the flow perturbations are defined as the disturbance relative to their Favre-averaged values.

Considering the schematic in Fig. 1, the flow field of IOIS can be decomposed to the combination of a passage-averaged time-mean value, the unsteady disturbance and a stationary passage-to-passage disturbance. If we consider the stationary disturbance as a "slowly moving" unsteady disturbance and its frequency is approaching zero, the flow field can be decomposed as a passage-averaged time-mean value  $\tilde{\phi}$  and an unsteady flow disturbance  $\phi''$ , whose frequency can be zero.

If the perturbation of a dummy variable  $\phi''$  can be represented as the harmonic form:

$$\phi'' = \sum_{l=1}^{l=N_h} \hat{\phi}_l (e^{I\omega_l t} + e^{-I\omega_l t}) \quad (1)$$

where  $l$  is the harmonic index,  $N_h$  is the number of harmonics,  $I$  is the imaginary unit  $\sqrt{-1}$ ,  $\omega_l$  is the angular frequency of the  $l^{\text{th}}$  harmonic and  $t$  is time. FNLH solves the coupled time-mean flow and the time-linearized harmonic flow perturbations. For simplicity, this coupled system can be represented symbolically in Equation 3 and detailed formulation can be found in ref [6, 14].

$$\mathbf{R}(\tilde{\mathbf{U}}) + \text{DF} = 0 \quad (2)$$

$$\sum_{l=1}^{l=N_h} \left( \frac{\partial \mathbf{R}}{\partial \mathbf{U}} \hat{\mathbf{U}}_l + I\omega_l \hat{\mathbf{U}}_l \right) = 0 \quad (3)$$

In Equation 3, DF is Deterministic Fluxes [17, 18], which represents the non-linear coupling between the mean flow and flow perturbations and can be directly computed using the Fourier modes [6].  $\hat{\mathbf{U}}_l$  is the  $l^{\text{th}}$  harmonic of conservative variable perturbations,

$I\omega_l \hat{\mathbf{U}}_l$  is the spectral source term,  $\frac{\partial \mathbf{R}}{\partial \mathbf{U}} \hat{\mathbf{U}}_l$  is the linearized flux in the harmonic form.  $\bar{\mathbf{U}}$  is the time-averaged conservative variables and it can be easily represented in terms of the Favre-averaged primitive variables, readers can refer to [6] for more details. Frozen turbulence is used in the current simulation and this approximation is found to produce satisfactory agreement with URANS for hot streak migrations in our previous work [14].

For the bladerow interface, DF is included in the mixing plane to conserve the time-averaged fluxes. To transmit disturbances to an adjacent bladerow, the mean flow is Fourier transformed and user-specified modes are transferred to adjacent bladerows. This is shown in Equation 4. For instance, the mean flow at the exit boundary of H01S is Fourier transformed and the modes are transferred to H01R to simulate H01S wake and the hot streak in H01R. On the other hand, to take into account the interaction of non-adjacent bladerow, the time-linearized flow is Fourier transformed and user-specified modes are extracted and transferred. This is shown in Equation 5. For instance, H01S wake and the hot streak is computed by the time-linearized solver in H01R, and at H01R exit, the time-linearized flow is Fourier transformed and the extracted modes are then transferred to I01S to simulate H01S wake and the hot streak in I01S. To transfer the hot streaks further into I01R, on the I01S exit boundary the linearized flow is Fourier transformed (see Equation 5) and the user-specified mode is transferred to I01R to faithfully represent the hot streaks in I01R.

$$\hat{\phi}_n = \frac{1}{P} \int_0^P \phi(\theta) e^{-I\lambda_n \theta} d\theta \quad \text{mean flow} \quad (4)$$

$$\hat{z}_n = \frac{1}{P} \int_0^P \hat{z}(\theta) e^{-I\lambda_n \theta} d\theta \quad \text{linearized flow} \quad (5)$$

In Equation 4 and 5,  $P$  is the pitch of the computational domain,  $\lambda_n$  is user-specified circumferential wave number,  $\phi(\theta)$  and  $\hat{z}(\theta)$  are the mean flow and linearized flow variables, respectively.  $\hat{\phi}_n$  and  $\hat{z}_n$  are the extracted Fourier modes with the specified circumferential wave number. For clarity, Equation 4 and 5 are described separately for mean flow and linearized flows. They can be essentially formulated into a unified approach to transmit any disturbances through a bladerow interface.

### Non-reflective Treatment and Its Regularization for Zero-Frequency Mode

The non-reflective treatment on the bladerow interface is an essential part in harmonic methods to minimize the attenuation of the disturbance when it is transferred from one blade row to the other. Previous studies of non-reflective treatment [19] show that a quasi-3D approach is more cost-effective compared to 1D and full 3D non reflective treatment. In this paper, we use the quasi-3D non-reflective treatment by Giles [20]. The mean flow is trivial to deal with and one can refer to Saxer and Giles [21] for more details. The focus here is on the non-reflective treatment of the harmonic flow perturbations.

The detailed derivation of non-reflective treatment for the harmonic flow is out of the scope of this paper and readers can refer to

Ref [19,20,22] for details. The objective here is to highlight the issue of constructing the left eigenvector of the dispersion relation for zero-frequency modes with certain combination of blade counts. The left eigenvector of the dispersion relation for frequency  $\omega_l$  and circumferential wave number  $m$  can be written as:

$$\mathbf{L}(\omega_l, m) = \begin{bmatrix} 1 & 0 & 0 & -\frac{1}{a^2} \\ 0 & mu_t & \omega'_l & \frac{m}{\rho} \\ 0 & \omega'_l & -mu_n & \frac{\omega'_l \psi}{\rho a} \\ 0 & \omega'_l & -mu_n & -\frac{\omega'_l \psi}{\rho a} \end{bmatrix} \quad (6)$$

where  $u_n$ ,  $u_t$ ,  $\rho$ , and  $a$  are area-averaged flow quantities on a certain radial band of the boundary mesh, and they are normal velocity, tangential velocity, density and speed of sound, respectively.  $\omega'_l$  and  $\psi$  are defined as:

$$\omega'_l = mu_t + \omega_l \quad (7)$$

$$\psi = \sqrt{1 - \frac{(a^2 - u_n^2)m^2}{(r\omega'_l)^2}} \quad (8)$$

The eigenvectors for the two acoustic waves that travel downstream and upstream can be co-linear if  $\omega'_l$  is approaching zero. This is known as acoustic resonance and was studied by Kersken et al. [19] for the aeroelastic analysis of a low pressure turbine. In the current case,  $\omega_l$  can be zero, for instance, the fundamental mode of H01S wake in I01S domain has zero frequency. The circumferential wave number  $m$  is a linear combination of the blade counts and when the blade counts are a multiple of each other,  $m$  can also be zero. Therefore for  $\mathbf{L}(\omega_l, m)$ , apart from entries in the 1st row, all other entries reduce to zero.  $\mathbf{L}(\omega_l, m)$  is singular and the non-reflective treatment will fail for this mode. A remedy can be applied to add damping to the dispersion relation to prevent the left eigenvector from becoming singular. Kersken et al. [19] proposed subtracting a small imaginary part from  $\omega'_l$ , such as  $\omega'_l = \omega'_l - I\varepsilon$ , to deal with the situation of  $\omega'_l \approx 0$ . This approach is adopted here to deal with the situation when  $\omega'_l = 0$  and  $m = 0$  take place simultaneously.  $\varepsilon$  is a tuning parameter and it is set to be 0.001 [23], which is found to be robust for the current application.

## Multispool Kinematics

Figure 1 shows a diagram of HP and IP turbines. The hot streak is illustrated as a low Engine Order (EO) disturbance at H01S inlet. To model the hot streaks in a harmonic method, we need to derive the spatial-temporal modes of the hot streak across all blade rows. The obtained modes will be selected to set up the harmonic solver.

In general, assume the pitchwise variation (i.e. hot streak) of a flow variable  $\phi$  on the exit boundary of H01S can be decomposed into a set of Fourier modes in the reference frame of H01S. For simplicity, we only demonstrate the spatial and temporal modes of the hot streaks through the stages, similar procedures can be used for other disturbances and more details can be found in Tyler and Sofrin [24]. At H01S exit, the harmonic form of the hot streak can be represented as:

$$\phi = \sum_{-\infty}^{\infty} \hat{\phi}_m e^{I(mN_{hs}\theta_{H01S})} \quad (9)$$

$\theta_{H01S}$  is the coordinate in the circumferential direction with the unit of radian.  $N_{hs}$  represents the number of hot streaks in the circumferential direction.  $m$  is an integer and it represents the harmonic content of the hot streaks at H01S exit. Because the spatial pattern of the hot streaks are generally not simple sinusoidal shapes, several harmonics are required to have a good reconstruction of the hot streaks at H01S exit. For clarity and simplicity, the Fourier coefficient  $\hat{\phi}_m$  and the Euler number  $e$  are dropped in the following text, the representation of the hot streak can be simplified as

$$mN_{hs}\theta_{H01S} \quad (10)$$

Applying the coordinate transformation to Equation 10, the hot streak at H01R inlet can be represented as:

$$mN_{hs}\Omega_{H01R}t + mN_{hs}\theta_{H01R} \quad (11)$$

$\theta_{H01R}$  is the circumferential coordinate in the frame reference of H01R and  $\Omega_{H01R}$  is the rotational speed of H01R. It can be seen that the hot streak is now an unsteady disturbance in H01R. If we transform Equation 11 to the frame reference of I01S and also include

the scattered modes, which is caused by the modulation of the disturbance by the flow non-uniformity in H01R, we obtain the temporal and spatial mode of the hot streak at I01S inlet as:

$$-nN_{H01R}\Omega_{H01R}t + (mN_{hs} + nN_{H01R})\theta_{I01S} \quad (12)$$

where  $n$  is an integer and it represents the harmonic content of the scattered modes,  $N_{H01R}$  is the blade count of H01R,  $\theta_{I01S}$  is the circumferential coordinate in the frame reference of H01R. The harmonics related to  $m$  represent the clocking effect between the hot streak and I01S and their frequencies are zero.

It is clear from Equation 12 that in the frame reference of I01S the hot streak has the zero-frequency modes, the so-called clocking effect, and also the unsteady modes, which are related to the frequency  $N_{H01R}\Omega_{H01R}$ . The spatial modes are linear combination of the circumferential wave number of the hot streak and the blade count of H01R. A further coordinate transformation from I01S to I01R is applied to Equation 12 and include scattered modes again, we obtain:

$$\begin{aligned} &[nN_{H01R}(\Omega_{I01R} - \Omega_{H01R}) + (mN_{hs} + lN_{I01S})\Omega_{I01R}]t \\ &+ (mN_{hs} + nN_{H01R} + lN_{I01S})\theta_{I01R} \end{aligned} \quad (13)$$

where  $l$  is an integer and it represents the harmonic content of the scattered modes of the hot streaks, which is caused by the modulation of the flow non-uniformity in I01S,  $\theta_{I01R}$  is the circumferential coordinate in the frame reference of I01R,  $\Omega_{I01R}$  is the rotational speed of I01R.

Equation 13 shows that there are two fundamental temporal frequencies of the hot streak in I01R and they are related to the difference of the shaft speed of the HP and IP, and the shaft speed of the IP spool. In terms of spatial modes, the circumferential wave number of the hot streak in I01R is a linear combination of the circumferential wave number of the hot streak, the blade counts of H01R and I01S.

Equation 10 to Equation 13 also show that as the hot streak (or any disturbance with trivial spatial modes) is transported through a few blade rows, the composition of its temporal and spatial modes become more complicated. In a URANS computation, all these modes are computed, if they can be resolved by the selected time step, while in a harmonic method, i.e. FNLH, not all modes can be computed, otherwise the computational cost would be too high and harmonic method will not show a clear advantage over URANS in terms of computational efficiency. Numerically the degree of freedom (DOF) to compute for each harmonic is roughly the same but



their significance on the flow varies greatly. One advantage (or disadvantage in some sense) of harmonic method compared to URANS is that one choose to compute selected modes in the simulations, this feature can be used as an advantage and offer significant reduction in computational cost.

## CFD Solver

The proposed method has been implemented in the turbomachinery CFD solver AU3X [25]. AU3X uses the cell-centered finite volume scheme to solve the steady/unsteady/harmonic RANS equations implicitly on unstructured meshes. The code is second-order accurate in space and time. Implicit dual-time stepping is used for URANS computations [26]. Second-order convective fluxes are computed by Roe's approximated Riemann solver and Monotonic Upwind Scheme for Conservation Law (MUSCL) [27] is used for the upwind fluxes with the van Albada limiter. In the linearized flow solver, the flow perturbations, in terms of Fourier coefficients, are extrapolated from the cell center to the cell interface using the MUSCL scheme to achieve 2<sup>nd</sup> order spatial accuracy. The Wilcox  $k - \omega$  turbulence model [28] is used for turbulence modelling. Automatic wall treatment [29] is also implemented to deal with complex geometries so that simulations tend to be less sensitive to near-wall grid spacing. The robustness of this treatment was demonstrated by the previous work on simulating multistage compressors at off-design conditions [30]. Newton's method is used to drive the solution to convergence iteratively via pseudo time-marching. For each pseudo time step, the coupled linear system of the time-mean flow and the time-linearized flow is solved by matrix-based GMRES, which is pre-conditioned with the additive Schwarz method [31]. The implementation is facilitated by using the PETSc [32] library.

## Results

Two test cases are used to demonstrate the capability of FNLH for multispool simulations. In the first test case, we demonstrate the capability of FNLH to correctly transmit a sinusoidal disturbance through computational domains with multiple rotational speeds. FNLH results will be compared with analytical solutions. In the second test case, FNLH is used to predict the hot streak migration in a full 3D two-stage multi-spool turbine in a three-shaft turbofan engine. The results are validated against URANS data. As FNLH can be considered as a reduced model of URANS, validation against URANS is sufficient in the 2nd test case to demonstrate that FNLH can be a computationally efficient alternative to URANS to simulate hot streak migrations in a multispool turbine.

### Case Study - Transmitting Sinusoidal disturbance in Multispool Ducts

The first test case is to verify the bladerow interface treatment of FNLH in a multispool setting by transmitting a disturbance through 4 ducts. The schematic of the computational domain is shown in Fig. 2 and only one passage for each duct is required for FNLH simulations. All the ducts have the same axial length and the number of repetitive sectors of the ducts are 8:64:16:112. This is the same as the multi-spool turbine case in the next section. Duct 1 and duct3 are stationary. Duct2 and duct4 are rotating but in the

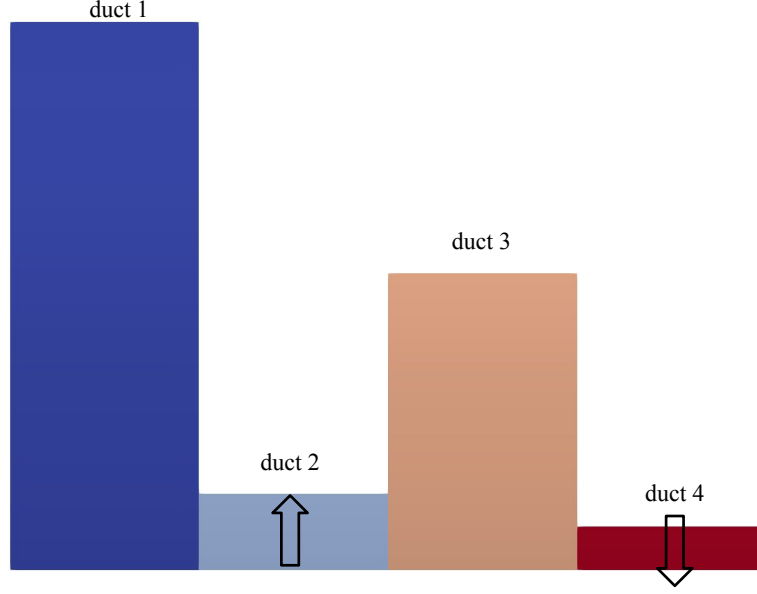


**FIGURE 2.** Schematic of 4 ducts with multiple rotational speeds

opposite direction, the ratio of their rotational speeds are -1.4, which is also similar to the multi-spool turbine case in the next section. A sinusoidal temperature disturbance is specified at the inlet of duct 1 with a wavelength equal to the pitch of Duct 1. This temperature disturbance will be transported downstream by a uniform background flow. The temperature of the background flow is 288k and the temperature perturbation at the inlet of Duct 1 is 10% of the background flow temperature. The background flow and the rotational speeds of duct 2 and duct 3 are chosen in such a way that the reduced frequency  $\beta$  in duct 2 is 1 and  $\beta$  is 1.4 in duct 4. The definition of  $\beta$  reads:

$$\beta = \frac{\omega/2\pi}{u_x/C_x} \quad (14)$$

Where  $\omega$  is the angular frequency of the unsteadiness, which is related to the rotational speeds of the duct 2 and duct 4,  $u_x$  is the axial velocity and  $C_x$  is the length of the duct.

Two background flows are used, one is axial and the other one has a flow angle of  $45^\circ$ . Each duct is meshed with structured grid and has similar grid spacing. Figure 3 shows the temperature contours at these two background flow configurations. Qualitatively the disturbance is transmitted downstream without attenuation. As the disturbance is transported by a uniform background flow, an analytical solution of the temperature profile at the exit of duct 4 is available. For the background flow with axial velocity, the temperature profile at the exit of duct 4 should be the same as the one as the inlet of duct 1. For the background flow with a flow angle of  $45^\circ$ , the temperature

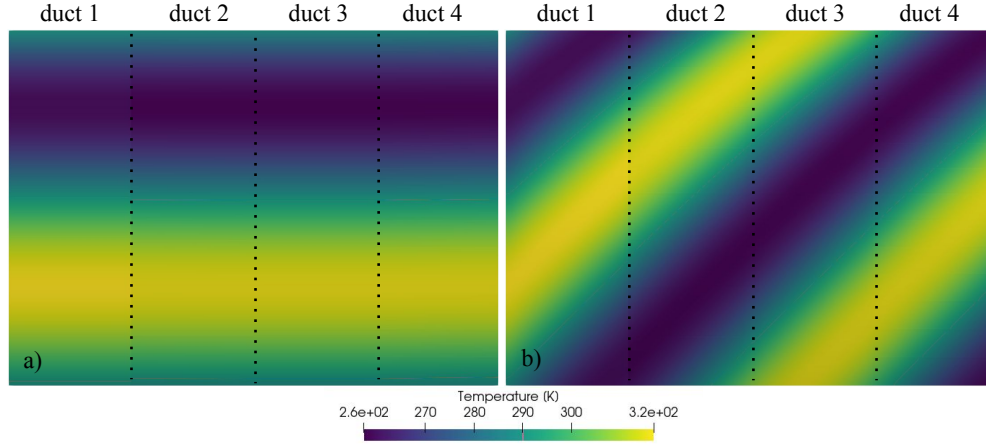


**FIGURE 3.** Temperature distribution with flow angle of a)  $0^\circ$  . b)  $45^\circ$

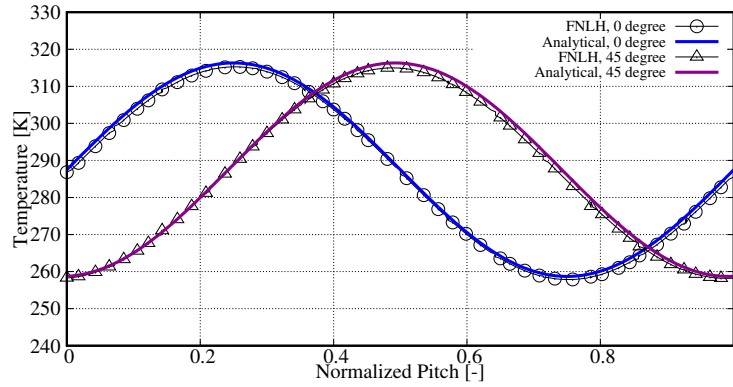


**FIGURE 4.** Temperature distribution at the exit of duct 4.

at the exit of duct 4 can be derived analytically by applying a phase shift of the one at the inlet of duct 1. Figure 4 shows the temperature profile at the exit of duct 4 for both background flows. There is excellent agreement between FNLH and the analytical solutions. The largest discrepancy is within 0.3% compared to analytical solution and this is caused by the numerical dissipation, especially for the  $45^\circ$  case, as the flow is not aligned with the grid any more.

### Case Study - Hot Streak Migration in HP and IP Turbines

The second test case is an industrial application and we demonstrate FNLH multispool capability by tracing the hot streak migration through the contra-rotating HP and IP turbines of a three-shaft turbofan engine. The meridional view of the geometry is shown in Fig. 5 a). The industrial relevance of this computation is that, the designers would like to have an efficient way to predict how the hot streaks are transmitted downstream so that they can improve the turbine aerothermal designs and also compute a realistic boundary conditions for the downstream low pressure turbines.

The area-averaged mean temperature  $\bar{T}_{in}$  at H01S inlet is representative of the engine at the take-off condition. 8 hot streaks are

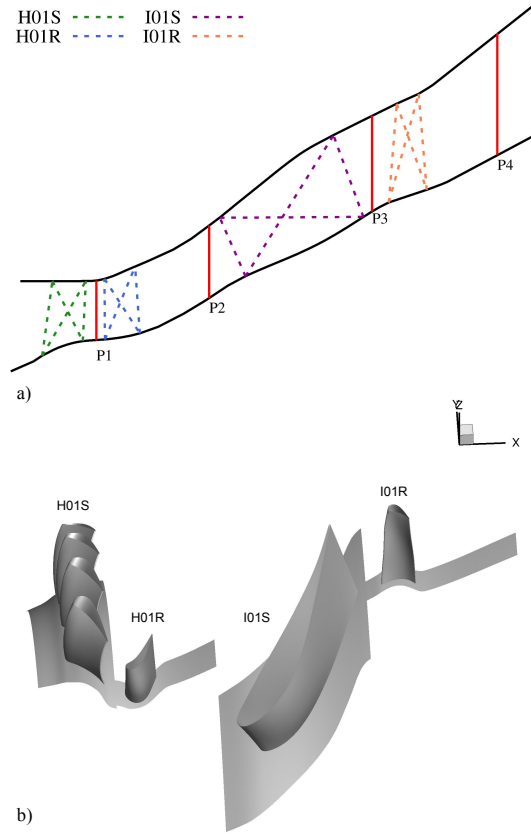


**FIGURE 5.** a) Meridional view of HP and IP Turbines. b) Computational domains of FNLH

distributed evenly in the circumferential direction, which is representative of industrial gas turbine applications. The combustion process is rich-burn and no swirl is prescribed at the inlet. The hot streak is therefore idealized as a Gaussian distribution of temperature in the  $r - \theta$  plane at H01S inlet and it can be defined as:

$$T(r, \theta) = \Delta T e^{-\frac{1}{2} \left( \frac{(\theta - \theta_c)^2}{\sigma_\theta^2} + \frac{(r - r_c)^2}{\sigma_r^2} \right)} \quad (15)$$

$\theta_c$  and  $r_c$  are the coordinates of the geometrical center of a hot streak.  $\sigma_\theta$  and  $\sigma_r$  are the standard deviation in  $\theta$  and  $r$  directions, and they are set to 60% of H01S pitch and 15% of H01S span, respectively. Such choice of  $\theta_c$  and  $r_c$  is to allow an aggressive non-uniformity in the radial direction but a relative weak one in the circumferential direction, which is characteristic of modern gas turbine combustors.  $\Delta T$  in Equation 15 is roughly 11% of  $\bar{T}_{in}$  and this is comparable to previous experimental campaigns [33]. Figure 6 shows the resulting temperature distribution at H01S inlet. The values have been normalized by  $\bar{T}_{in}$  and this value is also used to normalize the temperatures

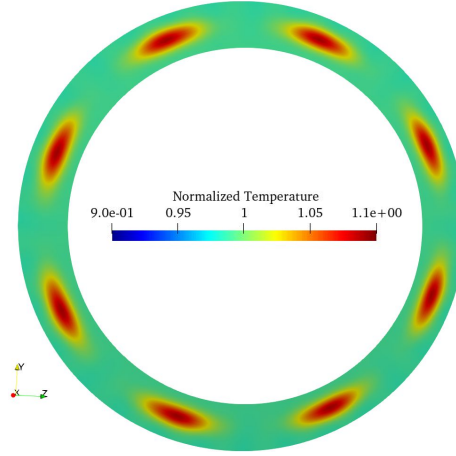


**FIGURE 6.** Demonstration of hot streaks at H01S inlet

in the following text.

### URANS Setup

With the original blade counts, a half annulus simulation is required for URANS simulations, therefore the blade counts have been slightly modified to the ratio of 2(H01S):8(H01R):1(I01S):7(I01R) so that a  $45^\circ$  sector can be modelled to reduce the computational cost of URANS. The ratio of the rotational speed of H01R and I01R is approximately -1.41:1.

For the URANS simulation, the period of the simulation is based on the lowest BPF, which is  $|\Omega_{I01R}|$  and is related to BPF of the hot streaks in I01R. Here we denote the period of the hot streak passing I01R in this  $45^\circ$  sector as  $\tau_{hs}$ . The time step is based on the highest BPF, which is  $|\Omega_{H01R}| + |\Omega_{I01R}|$ . This is because IP and HP spools are contra-rotating. 64 steps are used to resolve the BPF of I01R and H01R. From the above two time scales, we use 2162 time steps for one revolution of this  $45^\circ$  sector. This corresponds to more than 150 steps for the highest BPF of neighbouring blade rows and is sufficient compared to previous numerical study of hot streak migrations [34]. The URANS simulation is performed with  $5\tau_{hs}$  before sampling the solution for one  $\tau_{hs}$ .

### FNLH Setup

For FNLH simulations, 4 passages of H01S are used to model the hot streaks and only one passage is required for the rest of the bladerows. This is shown in Fig. 5 b). The comparisons with URANS simulation in terms of computational domains are summarized in Table 1. With the current FNLH setup, the reduction of number of passages to compute compared to URANS is 4 and for the original blade counts which requires a  $180^\circ$  sector simulation, the reduction would be around 16. It is possible to use just one H01S passage in the FNLH simulation by performing a Fourier transform of the hot streaks and solve these Fourier modes with zero-frequency in H01S, but this does not necessarily reduce the actual DOF in the computations, since the computation of one harmonic is roughly twice the DOF of computing a steady solution and a few harmonics (e.g. 6) are required to represent the hot streaks.

**TABLE 1.** Number of passages in URANS and FNLH simulations for each bladerow

	H01S	H01R	I01R	I01S
URANS	4	8	2	14
FNLH	4	1	1	1

**TABLE 2.** FNLH setup for hot streak migration

Bladerow	Temporal mode	Spatial mode	Note
H01S	$-iN_{H01R}\Omega_{H01R}, i \in [1 : 2]$	$iN_{H01R}, i \in [1 : 2]$	exit, H01R potential field
H01R	$iN_{H01S}\Omega_{H01R}, i \in [1 : 4]$	$iN_{H01S}, i \in [1 : 4]$	inlet, H01S wake
	$mN_{hs}\Omega_{H01R}, m \in [1 : 6]$	$mN_{hs}, m \in [1 : 6]$	inlet, hot streak
	$iN_{I01S}\Omega_{H01R}, i \in [1 : 2]$	$iN_{I01S}, i \in [1 : 2]$	exit, I01S potential field
I01S	$iN_{H01R}\Omega_{H01R}, i \in [1 : 4]$	$iN_{H01R}, i \in [1 : 4]$	inlet, H01R wake
	$m \times 0, m \in [1 : 6]$	$mN_{hs}, m \in [1 : 6]$	inlet, hot streak
	$-iN_{I01R}\Omega_{I01R}, i \in [1 : 2]$	$iN_{I01R}, i \in [1 : 2]$	exit, I01R potential field
I01R	$iN_{I01S}\Omega_{I01R}, i \in [1 : 4]$	$iN_{I01S}, i \in [1 : 4]$	inlet, I01S wake
	$mN_{hs}\Omega_{I01R}, m \in [1 : 6]$	$mN_{hs}, m \in [1 : 6]$	inlet, hot streak

For multispool simulations, FNLH is set up in two steps. The first step is for adjacent row interactions. 4 harmonics are used to compute the wake interaction from upstream and 2 harmonics are used to take into account the potential effect from downstream. The second step is to set up the multirow interactions. Multirow interactions contribute to the transfer of the hot streaks through HP and IP turbines. The spatial and temporal mode representation of the hot streaks in I01S and I01R have been described by Equation 12 and Equation 13. The hot streaks is a low EO disturbance and decays slowly in the streamwise direction. In this work, we only compute the fundamental modes  $m$  which is related to its circumferential wave number at H01S inlet and ignore all the scattered modes which are related to circumferential wave number  $n$  and  $l$ , as is shown in Equation 12 and Equation 13. 6 harmonic modes are used to simulate the hot streaks in H01R, I01S and I01R.

The complete setup of FNLH for this hot streak migration simulation is summarized in Table 2.  $i$  refers to the harmonic index for adjacent row interactions and  $m$  for the harmonic index of the hot streaks in multirow interactions. In the "Note" column, it states which boundary the harmonic perturbations are specified and what physical field the harmonics are trying to reconstruct. The rationale of such setup is based on the observation in the previous work [6, 9, 18] that DF in the mean flow is dominated by the harmonics related to adjacent row interaction. Apart from modelling the hot streaks, all other stator-stator or rotor-rotor interactions are ignored in this setup. This choice of mode selection will be verified against URANS data in the following text.

## Mesh Configuration

In-house multi-block structured grid generator [35] is used to mesh the turbine blade passages. 70 layers are used in the span-wise direction and 200 points are placed on the blades in the blade-to-blade section. This leads to roughly 0.9 million cells in each passage and the average  $y^+$  on the wall is roughly 1. Identical meshes are used for steady and FNLH simulations. The meshes for each blade passage are replicated in the circumferential direction to generate the mesh for the URANS simulation. Since the same mesh resolution and spatial discretization are used for URANS, mixing plane and FNLH, the difference in the results are only caused by the modelling fidelity of unsteady blade row interactions in steady mixing plane, FNLH and URANS simulations.

## Boundary Conditions

For steady/FNLH/URANS simulations, at the inlet of H01S, total pressure, total temperature, yaw and swirl flow angles are specified and in the current simulation no swirl is prescribed at the inlet. At the exit of I01R, static pressure is used. With respect to bladerow interface, for steady/FNLH, quasi-3D non-reflective treatment are used and for URANS, sliding planes are applied.

## FNLH Predicted Temperature Traverse

Figure 7 shows the temperature and entropy distribution around the middle span for FNLH and URANS. It can be seen that FNLH data match well with URANS solutions qualitatively. Due to the large temperature ratio across the turbine stages, the variation of temperature from H01S inlet to I01R exit is much larger than the temperature variation in the circumferential direction. The trace of the hot streaks can be indirectly illustrated by the entropy distribution. Since entropy perturbation can be written as  $ds = C_p \frac{dT}{T} - R \frac{dp}{p}$ . If we take  $T$  and  $P$  as the circumferential averaged temperature and pressure, respectively, and  $dp$  is normally much smaller than  $P$ , there is approximately a linear relation between temperature and entropy variations, i.e.  $ds \approx C_p \frac{dT}{T}$ .

The predicted circumferential temperature variations are compared at 4 axial locations against URANS data and this is shown in Fig. 8. These 4 axial locations are labelled as P1,P2,P3 and P4 and their locations are illustrated in Fig. 5 a). A 45° sector is conducted for the URANS simulation but here a half annulus solution is plotted to demonstrate the circumferential migration of the hot streak on these 4 planes. In Fig. 8 the FNLH solutions match well with URANS data in terms of circumferential and radial migration of the hot streaks at these 4 planes. The largest circumferential migration of the hot streak is from P2 to P3 plane. This is because the solidity of I01S is much lower than H01R and H01S and the chord is also larger, for the same amount of turning, the hot streak will migrate more in the circumferential direction. It is also interesting to notice that the hot streaks also migrate towards the hub and this is captured well by the FNLH solution.

Quantitative comparisons of the temperature distributions at these 4 planes are shown in Fig. 9, Fig. 10 and Fig. 11, which are extracted at 50%, 25% and 75% spans. The temperatures are shown on a circumferential variation of 90°, which encloses two hot streaks. FNLH solutions are found to match very well with URANS data and it is remarkable to observe that on P4, the low EO variation

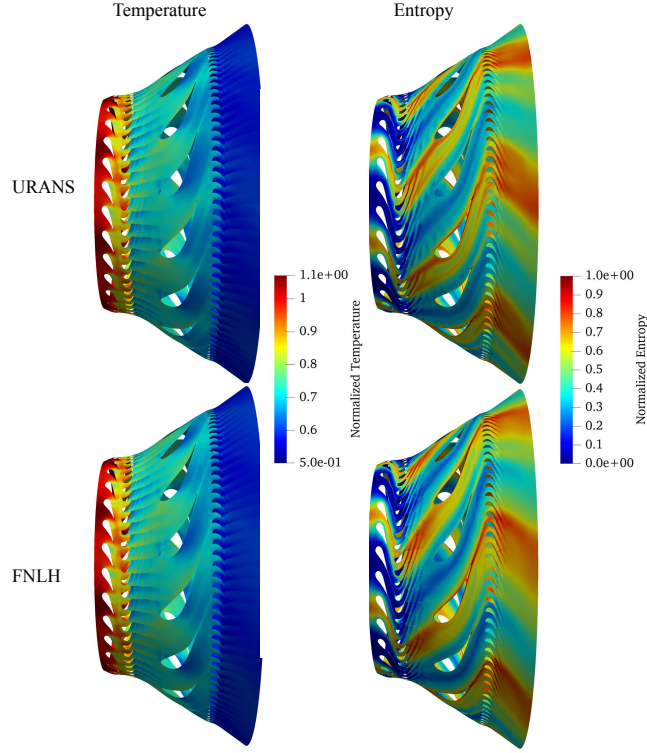


**FIGURE 7.** Instantaneous distribution of temperature (Left) and entropy (right) on the middle span of HP and IP turbines.

of the temperature due to the hot streak from H01S inlet is captured very well at downstream I01R TE by FNLH by only using its fundamental modes which is related to  $m$  from Equation 11 to Equation 13.

From Fig. 10 and Fig. 11, it is also interesting to notice that the radial migration of the hot streaks towards the hub are also captured accurately by FNLH. At H01S inlet, the hot streaks are centered around the mid-span. Upstream of H01R leading edge, the temperature circumferential variation at 25% span is slightly larger than the one at 75% span. However, significantly more temperature variation is observed upstream I01R LE at 25% span position while the one at 75% span is much smaller. In fact the temperature variation at 25% span at this axial location is slightly larger than the one at the middle span (see Fig. 9).

A more detailed quantitative comparison of the temperature distribution at 25% and 50% spans of P4 is shown in Figure 12 by breaking down the temperature fluctuation into Fourier modes of different circumferential wave number. It can be seen that the circumferential temperature perturbation is dominated by low EO modes which are related to the hot streaks. FNLH solutions have very good agreement with URANS data on these dominant modes (e.g. 8 and 16). It is interesting to see that mode 24 is underestimated by FNLH compared to other modes. This is probably because cross-coupling of the harmonics are not taken into account in the current harmonic solution. Figure 12 also shows clearly that the temperature fluctuation at 25% span is comparable to the one at 50% span, which is due to the radial migration of the hot streaks towards the hub.

Regarding to the radial migration of the hot streaks towards the hub, this was reported by Bulter et al. [36] experimentally. Bulter et



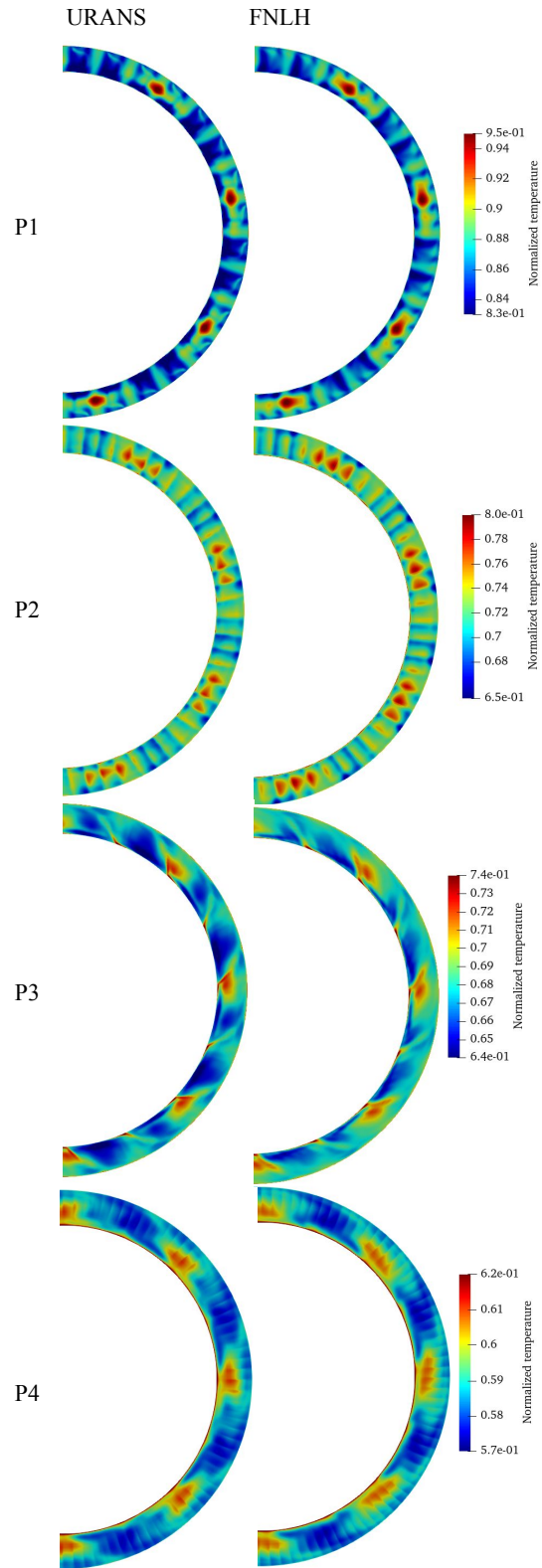


**FIGURE 8.** Instantaneous temperature distribution at selected 4 axial planes

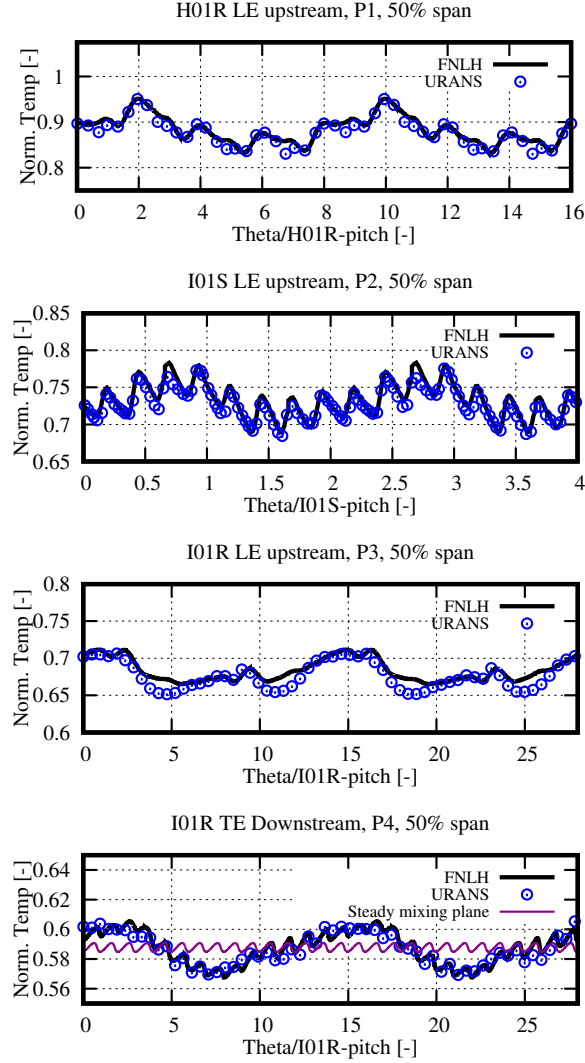


**FIGURE 9.** Circumferential distribution of instantaneous temperature distribution at 50% on the selected axial planes

al. [36] considered such radial migration was due to the secondary flow effect, which was demonstrated analytically by Lakshminarayana and Horlock [37] using inviscid secondary flow theory and also the segregation effect observed by Kerrebrock and Mikolajczak [38]. Later on, Shang and Epstein [39] had numerically predicted the radial migration of the hot streaks towards the hub and attribute the cause of such radial migration to the buoyancy effects. He et al. [34] also numerically predicted the radial migration of the hot streaks towards the hub for the MT1 stage. In He's simulation, there seemed to be stronger secondary flows towards the hub than the tip regions due to passage-vortex and the radial migration might be, to some extent, attributed to the buoyancy effect. The above previous work were undertaken on a single stage turbine. Based on the results of this work, the phenomenon that hot streaks migrate radially towards the hub is also observed for contra-rotating multispool turbines. Furthermore, such phenomenon can be captured by the FNLH method using only a fraction of the cost of the URANS simulation. A detailed investigation of the mechanism of hot streak migration towards

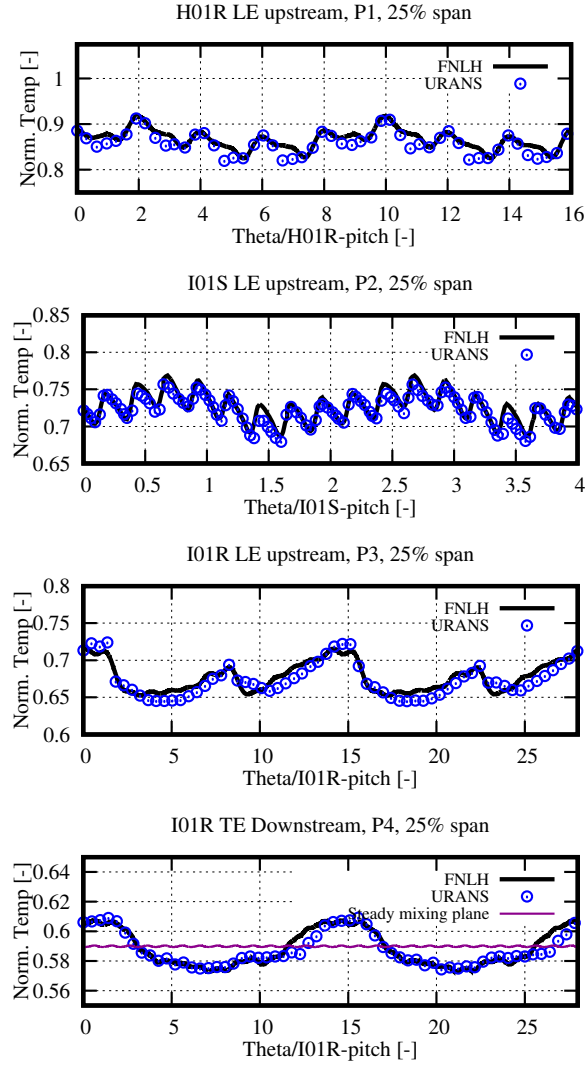


**FIGURE 10.** Circumferential distribution of instantaneous temperature distribution at 25% on the selected axial planes

the hub is out of the scope of this paper and this will be addressed in future publications.

On plane P4, which is downstream I01R TE, the steady mixing plane solution is also plotted in Fig. 9, Fig. 10 and Fig. 11. It can be seen that the low EO circumferential temperature fluctuation by the hot streaks is significantly larger than the blade-to-blade temperature variations. The steady mixing plane solution is only able to capture the latter and therefore fails to predict a correct temperature variation at I01R exit.

The effectiveness of the quasi-3D non-reflective treatment of the time-linearized flow can be demonstrated by the FNLH predicted temperature traverse downstream I01R TE and this is shown in Fig. 13. It can be seen that the agreement with the URANS data is improved by applying the quasi-3D non-reflective treatment to the time-linearized flow. However, it is noted that the non-reflective treatment to the mean flow is still applied even if the one for the time-linearized flow is not used..

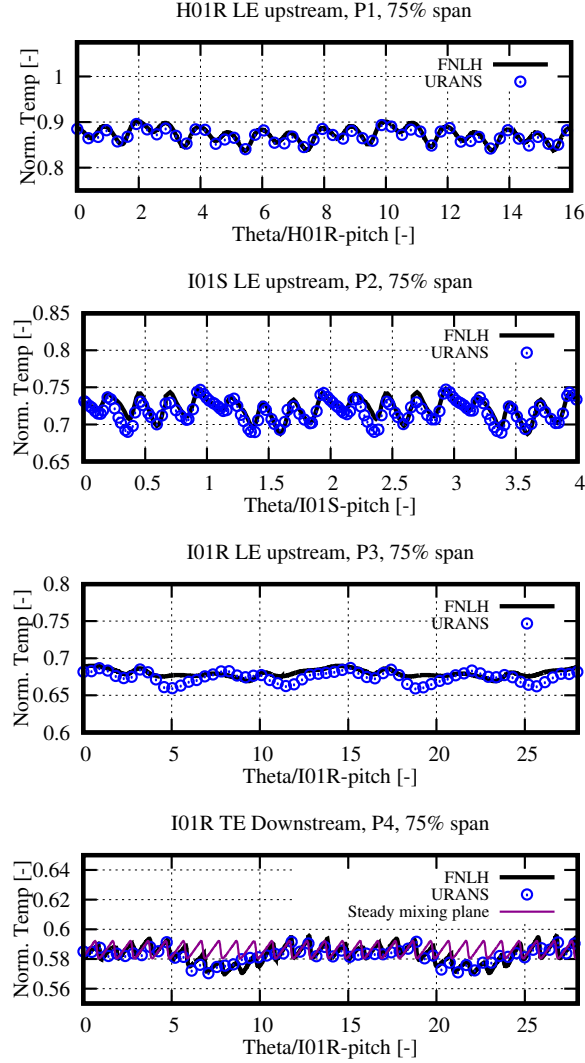


**FIGURE 11.** Circumferential distribution of instantaneous temperature distribution at 75% on the selected axial planes

In Fig. 7, entropy is used to illustrate the migration of the hot streaks, besides it also shows the propagation of the wakes of the bladerows to the downstream. A quantitative comparisons of the wake propagation with the URANS data on the middle span slice is shown in Fig. 14. For each location, the entropy is normalized by subtracting the minimum value and then divided by the maximum variation in the circumferential direction, and the minimum values and the maximum variation are taken from the URANS data. It can be seen that at H01R LE, the wake is captured accurately. As we move downstream, the overall shape of the wake is captured very well but discrepancies are still visible. This is mainly caused by the fact that the scattered modes of the hot streaks are not computed in I01S and I01R (see Table 2). As is shown in the previous text, satisfactory agreement with URANS data on the temperature traverse is obtained using the FNLH setup in Table 2. Adding more harmonics can improve the solutions but also lead to more expensive computations. An optimal configuration of the harmonics should strike the best balance between accuracy and computational speed and this will be

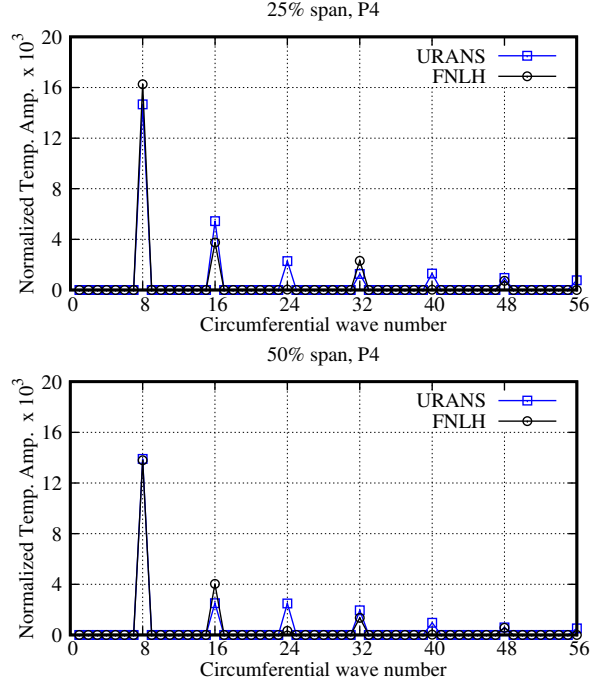


**FIGURE 12.** Fourier decomposition of circumferential temperature distribution at P4.

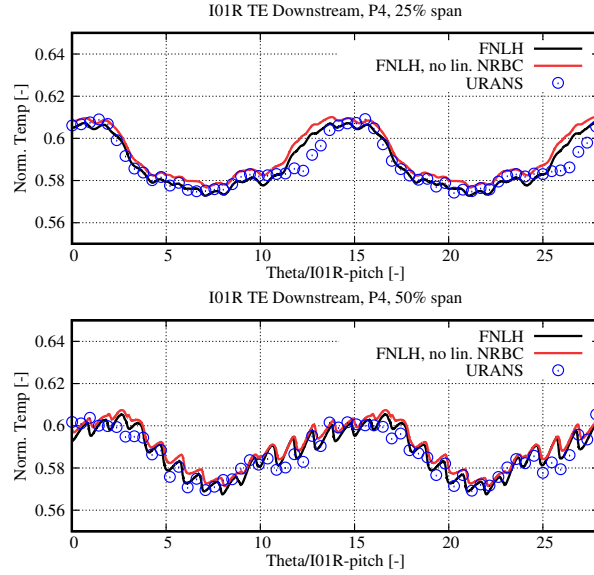


**FIGURE 13.** Effect of the quasi-3D non-reflective treatment of the time-linearized flow on the FNLH predicted temperature traverse at P4.

explored in the future work.

Equation 3 shows that the time-mean flow field will differ from a steady simulation due to the presence of DF. Figure 16 shows the Favre-averaged temperature distribution on P4 plane for URANS. FNLH and steady mixing plane produce single passage solutions and their solutions are replicated in the circumferential direction to be compared with URANS data. Strictly speaking,  $\Omega_{I01R}$  and  $\Omega_{H01R}$

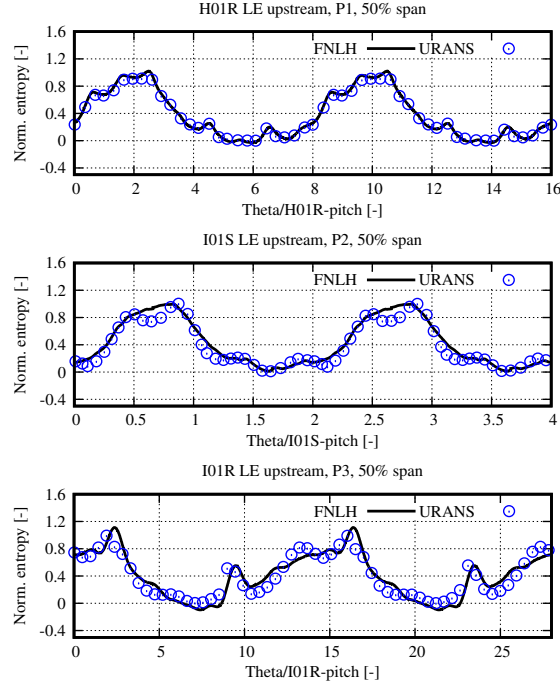


**FIGURE 14.** Wake profiles around the middle span at P1, P2 and P3 planes.

are not rational multiples of one another, the flows in I01R will never reach a full periodic state. However, the unsteady flow in I01R is dominated by the I01S-I01R and hot-streak-I01R interactions, H01R-I01R interaction is of secondary importance. The time-mean flow of I01R is produced by performing Favre-averaging over one  $\tau_{hs}$  for primitive variables.

It can be seen in Fig. 15 that there is good agreement between FNLH and URANS solutions, steady mixing plane solution is rather different from the former two. FNLH/URANS solutions show more mixing towards the hub. As is described in the previous text, the radial migration of the hot streaks towards the hub can be due to the unsteady secondary flows around the hub. Such unsteady flow contributes to DF in the mean flow and leads to more mixing in span and circumferential direction.

Fig. 16 shows the distribution of Favre-averaged temperature in the circumferential direction at 25%, 50% and 75% span on plane P4. Since the flows are periodic from passage-to-passage for FNLH and mixing plane solutions and almost periodic for URANS, solutions of two I01R passages are reconstructed and compared. It can be seen that FNLH shows significant improvement over mixing plane solution compared to URANS data. Steady mixing plane solutions are more similar to FNLH/URANS solutions at the middle span but has more discrepancies towards the endwalls, in particular towards the casing. The explanation is that this is due to the unsteady secondary flows caused by the hot streaks and upstream wake towards the endwalls. This generates DF in the mean flow system and leads to more mixing. As blades are more loaded towards the casing, this generates stronger unsteady effects in the corresponding regions of downstream bladerows, this leads to more discrepancies between FNLH/URANS and mixing plane solutions, as is shown in the 75% span solution of Fig. 16.

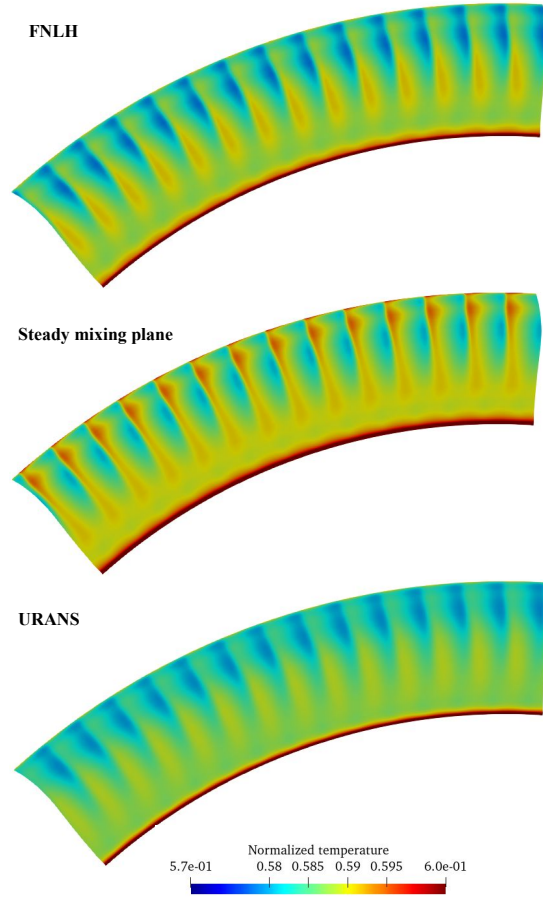


**FIGURE 15.** Favre-averaged temperature at P4 plane

**TABLE 3.** Comparison of adiabatic efficiency by URANS, FNLH and mixing plane

	URANS	FNLH	MP
$\eta$	reference	$-0.2\%$	$+0.9\%$

Table 3 shows the adiabatic efficiency  $\eta$  computed by URANS, FNLH and mixing plane, respectively. The URANS data is taken as the reference. The FNLH and mixing plane data are expressed as the difference to this reference value. The URANS shows a lower efficiency than the mixing plane computation. This can be explained by the unsteady wake recovery effect in turbomachines [40,41]. In a compressor passage, the wake is stretched when it is transported downstream, while in a turbine passage it is compressed. When the wake is mixed out, in a compressor the stretched wake leads to lower loss while in a turbine the compressed wake yields higher loss. This trend is captured well by the FNLH result but such unsteady effect slightly over-predicted.

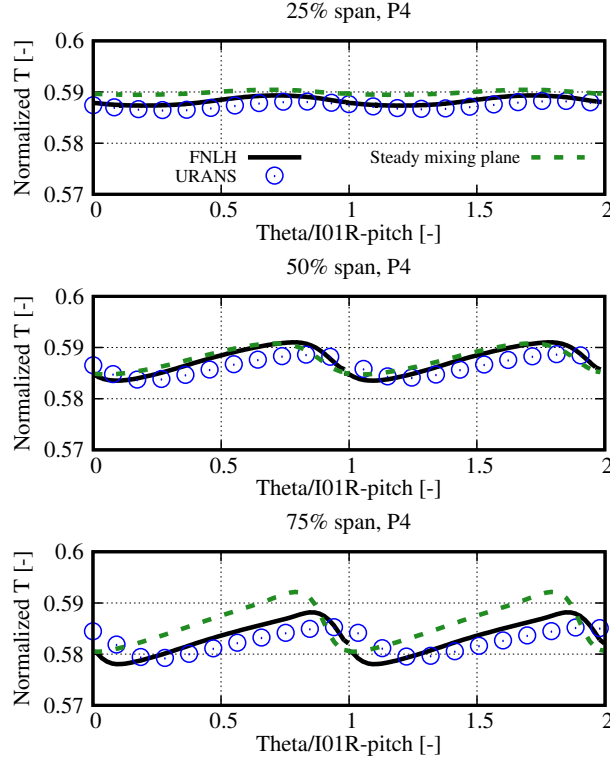


**FIGURE 16.** Favre-averaged temperature at 25%, 50% and 75% spans of P4 plane

### Computational Efficiency and Memory Usage of FNLH

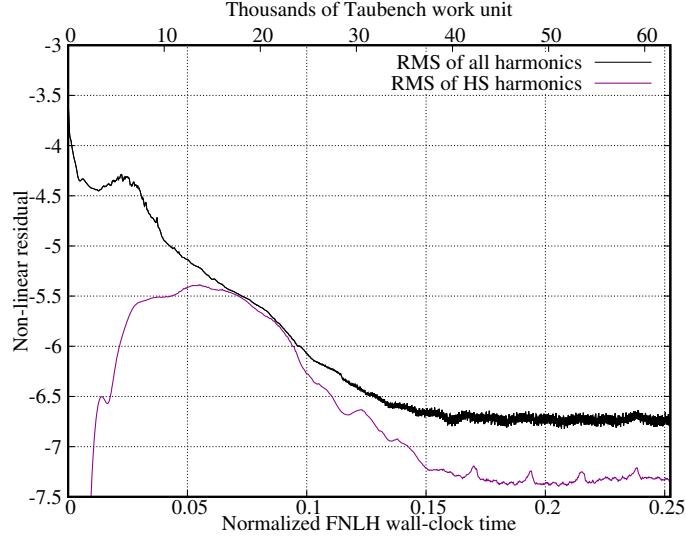
The computational efficiency of FNLH over URANS benefits from a significant reduction of the computational domain (see Table 1) and using convergence acceleration technique to drive the flow to periodic state significantly faster. Among the 4 bladerows of the multispool turbine case, I01R has the slowest convergence as its convergence can only be reached if the hot streak travels through H01S/H01R/I01S and reaches the exit boundary of I01R. The convergence history of I01R is shown in Fig. 17. The running time of FNLH is represented in two forms. The first one is in terms of the normalized time, which is the FNLH wall clock time normalized by the URANS running time for one revolution of the  $45^\circ$  sector. This URANS running time will be denoted as  $\tau_0$  in the following text for simplicity. The second one is in terms of TauBench Work Unit (WU), which shows the wall clock time of FNLH simulations. The running time of one WU is obtained by executing the command “`mpirun -np 1 ./TauBench -n 250000 -s 10`”<sup>1</sup>.

Figure 17 shows that the RMS of the residuals of all the harmonics and the harmonics related to the Hot Streak (HS) harmonics. It can be seen that the residuals related to HS are initially zero and they start rising as the computation proceeds, which indicates that the hot streaks has reached I01R. Figure 17 also shows that FNLH converges around 15% of  $\tau_0$ . Future work is planned to improve the quality of the Jacobian and the preconditioner to reach a deeper convergence.

The computational efficiency of FNLH can also be demonstrated by probing the FNLH solution. This is similar to URANS simulations

<sup>1</sup><https://how5.cenaero.be/content/guidelines>





**FIGURE 17.** Residuals of I01R for all the harmonics and the harmonics related to hot streaks.

where probes are used to monitor if the unsteady solution has reached a periodic state. Three probes are placed on P4 plane and they are located roughly at the mid-pitch location of 25%, 50% and 75% span positions. Figure 18 shows the RMS of the magnitude/phase of the harmonics related to the hot streak (solid line) and the harmonics related to I01S wake(dashed) line. The FNLH running time is normalized by  $\tau_0$ . It can be seen that the phase and magnitudes converges within 15% of the  $\tau_0$ . This is consistent with the convergence history shown in Fig. 17.

In the current URANS simulation, 5 revolutions are used before unsteady flows are sampled. The observation in Fig. 17 and Fig. 18 strongly indicates that FNLH can have a reduction of wall-clock time by roughly 30x compared to URANS for this 45° sector. If the whole annulus is the case, a reduction of 240 is expected.

As is shown in Table 1, in the FNLH computation, one passage is required for H01R, I01S and I01R, and 4 passages are used for NGV. For the harmonic setup in Table 2, the implementation of FNLH in the current CFD solver consumes roughly 56GB of RAM. This means one can run the FNLH simulation using a typical workstation.

## Conclusions

Multispool URANS simulations are more expensive compared to multistage simulations where all the components are on the same shaft, due to the disparity in the time scales that are involved in the simulation. This time disparity can be effectively removed by harmonic methods and this paper has extended the FNLH method to simulate unsteady multispool interactions efficiently, in particular, the migration of hot streaks through HP and IP turbines in a three-shaft turbofan engine at the take-off condition. 4 passages of NGV is used to model the hot streaks and for other bladerows, only one passage is required. GMRES is used to solve the coupled mean flow and harmonic flow perturbations, and this accelerates the flow to reach periodic state in the Fourier space.

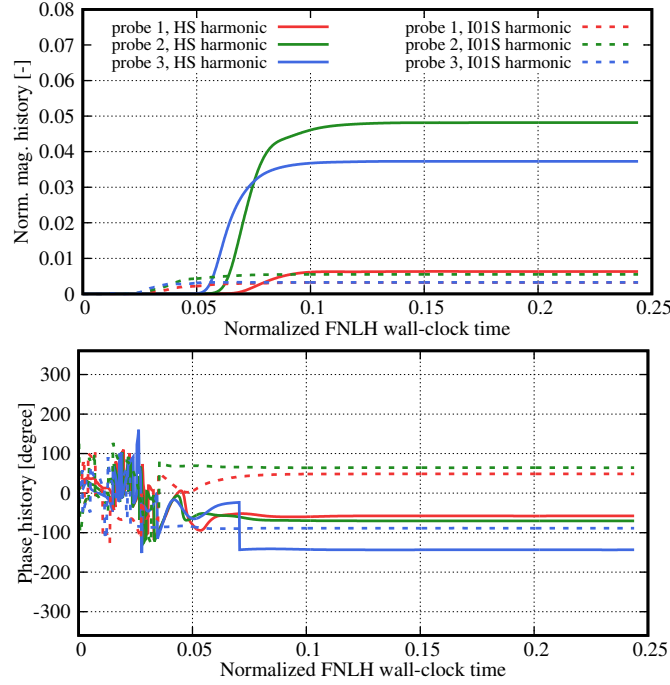


**FIGURE 18.** Probed harmonic solutions at P4 plane

Regularization of the left eigenvector of the dispersion relation is addressed for the non-reflective treatment to handle the situation when  $m$  and  $\omega'$  (Equation 6) both reach zero. In the current FNLH simulation, only the harmonics related to adjacent row interactions and fundamental modes of the hot streaks are included to strike a balance of accuracy and computational cost. Good agreement is observed to predict the migration of the hot streaks through HP and IP stages compared to URANS data.

The 4-duct case verifies the capability of FNLH blade-row interface treatment on transmitting disturbance in a multi-spool setting. In the multispool turbine simulations of this paper, hot streaks migrate towards the hub. Towards the exit of I01R, the circumferential temperature variation at 25% span is comparable to the one at the mid-span. Such radial migration towards the hub is captured very well by the FNLH method using only the fundamental modes of the hot streaks. Spectral analysis of the circumferential temperature variation confirms that the temperature fluctuation is dominated by the hot-streak related low EO modes and the FNLH-predicted dominant low EO modes also match very well with URANS data.

Compared to URANS simulations, the current FNLH simulation converges within 15% of the running time of  $\tau_0$ . This is roughly 30 times more efficient than the  $45^\circ$  sector URANS simulation which runs for 5 revolutions, and roughly 240 times more efficient than the whole annulus URANS. This work demonstrates that FNLH can be an efficient design tool to predict temperature traverses in multispool turbines.

Future work includes removing the assumption of frozen turbulence via a robust implementation of linearized turbulence models and improving the accuracy of FNLH by including the non-linear coupling of the harmonics. These will be addressed in future publications.

## ACKNOWLEDGMENT

The authors are grateful to Rolls-Royce plc and Aerospace Technology Institute for funding this work under the CORDITE project and granting permission for its publication. The authors would also like to thank Dr. John Adamczyk for discussion. This work used the Cirrus UK National Tier-2 HPC Service at EPCC (<http://www.cirrus.ac.uk>) funded by the University of Edinburgh and EPSRC (EP/P020267/1).

## NOMENCLATURE

### Latin symbols

- $a$  speed of sound  
 $C_x$  axial chord  
 $C_p$  specific heat at constant pressure  
 $I$  imaginary unit,  $\sqrt{-1}$   
 $l$  circumferential wave number, harmonic index  
 $L$  left eigenvector of the dispersion relation  
 $m$  circumferential wave number  
 $n$  circumferential wave number  
 $N$  number of passages  
 $N_h$  number of harmonics  
 $u$  velocity  
 $U$  conservative flow variable  
 $p$  pressure  
 $q$  primitive flow variable  
 $\mathbf{R}$  residual  
 $r$  radius  
 $s$  entropy  
 $t$  time  
 $T$  temperature

### Greek symbols

- $\beta$  reduced frequency  
 $\rho$  density  
 $\eta$  adiabatic efficiency

$\theta$  angle  
 $\lambda$  circumferential wave number in Fourier transform  
 $\sigma$  standard deviation in normal distribution  
 $\tau$  time  
 $\phi$  dummy flow variable  
 $\psi$  dummy flow variable  
 $\omega$  angular frequency  
 $\Omega$  shaft rotational speed

### Subscripts, superscripts and operators

$i$  spatial index  
 $j$  spatial index  
 $k$  space navigation index  
 $l$  Fourier index  
 $'$  fluctuation relative to the passage-averaged quantity  
 $''$  fluctuation relative to the Favre-averaged quantity  
 $-$  time-average  
 $\sim$  Favre-average  
 $\wedge$  Fourier coefficient

### Acronym

CFD Computational Fluid Dynamics  
 CPU Central Processing Unit  
 DF Deterministic Flux  
 DOF Degree of freedom  
 EO Engine Order  
 FNLH Favre-averaged Non-Linear Harmonic  
 GPU Graphics Processing Unit  
 HB Harmonic Balance  
 HS Hot streak  
 IBPA Inter-Blade Phase Angle  
 MUSCL Monotonic Upstream-centered Scheme for Conservation Laws  
 NGV Nozzel Guide Vane

NLH Non-Linear Harmonic

NS Navier-Stokes

RANS Reynolds-Averaged Navier-Stokes

RMS Root-mean-square

URANS Unsteady Reynolds-Averaged Navier-Stokes

WU Work unit

## REFERENCES

- [1] Hall, K. C., and Crawley, E. F., 1989. "Calculation of unsteady flows in turbomachinery using the linearized Euler equations". *AIAA Journal*, **27**(6), June, pp. 777–787.
- [2] Clark, W. S., and Hall, K. C., 1999. "A time-linearized navier–stokes analysis of stall flutter". *Journal of Turbomachinery*, **122**(3), Feb., pp. 467–476.
- [3] Hall, K. C., and Ekici, K., 2005. "Multistage coupling for unsteady flows in turbomachinery". *AIAA Journal*, **43**(3), Mar., pp. 624–632.
- [4] Hall, K. C., Thomas, J. P., and Clark, W. S., 2002. "Computation of unsteady nonlinear flows in cascades using a harmonic balance technique". *AIAA Journal*, **40**(5), May, pp. 879–886.
- [5] He, L., and Ning, W., 1998. "Efficient approach for analysis of unsteady viscous flows in turbomachines". *AIAA Journal*, **36**(11), Nov., pp. 2005–2012.
- [6] Wang, F., and di Mare, L., 2019. "Favre-averaged nonlinear harmonic method for compressible periodic flows". *AIAA Journal*, **57**(3), mar, pp. 1133–1142.
- [7] Vasanthakumar, P., 2003. "Three dimensional frequency-domain solution method for unsteady turbomachinery flows". Phd thesis, Durham University, Durham, UK, Jan.
- [8] Vilmin, S., Lorrain, E., Debrabandere, F., Tartinvill, B., Capron, A., and Hirsch, C., 2013. "The nonlinear harmonic method applied to the combined effects of multi-row unsteady flows". In Volume 6C: Turbomachinery, American Society of Mechanical Engineers.
- [9] Wang, F., di Mare, L., and Adami, P., 2019. "Favre-averaged fourier-based methods for gas turbine flows". In Volume 2C: Turbomachinery, American Society of Mechanical Engineers.
- [10] Wang, F., and di Mare, L., 2020. "Efficient approach for simulating aperiodic flows due to geometry distortions". *AIAA Journal*, **58**(3), Mar., pp. 1278–1291.
- [11] Wang, F., and di Mare, L., 2021. "Analysis of transonic bladerows with non-uniform geometry using the spectral method". *Journal of Turbomachinery*, **143**(12), July.

- [12] Frey, C., Ashcroft, G., Kersken, H.-P., and Voigt, C., 2014. "A harmonic balance technique for multistage turbomachinery applications". In Volume 2B: Turbomachinery, American Society of Mechanical Engineers.
- [13] He, L., Chen, T., Wells, R. G., Li, Y. S., and Ning, W., 2002. "Analysis of Rotor-Rotor and Stator-Stator Interferences in Multi-Stage Turbomachines". *Journal of Turbomachinery*, **124**(4), 11, pp. 564–571.
- [14] Wang, F., and di Mare, L., 2022. "Computation of multistage flows using a fourier approach". *AIAA Journal*, **60**(1), pp. 345–359.
- [15] Romagnosi, L., Li, Y., Mezine, M., Teixeira, M., Vilmin, S., Anker, J. E., Claramunt, K., Baux, Y., and Hirsch, C., 2019. "A methodology for steady and unsteady full-engine simulations". In Volume 2C: Turbomachinery, American Society of Mechanical Engineers.
- [16] Favre, A., 1965. The equation of compressible turbulent gases. Tech. Rep. AD0622097, Aix-Marseille University, jan.
- [17] Adamczyk, J. J., 2000. "Aerodynamic analysis of multistage turbomachinery flows in support of aerodynamic design". *Journal of Turbomachinery*, **122**(2), p. 189.
- [18] Wang, F., Carnevale, M., and di Mare, L., 2018. "Numerical Study of Deterministic Fluxes in Compressor Passages". *Journal of Turbomachinery*, **140**(10), 09.
- [19] Kersken, H.-P., Ashcroft, G., Frey, C., Wolfrum, N., and Korte, D., 2014. "Nonreflecting boundary conditions for aeroelastic analysis in time and frequency domain 3d RANS solvers". In Volume 2B: Turbomachinery, American Society of Mechanical Engineers.
- [20] Giles, M., 1988. Non-reflecting boundary conditions for the euler equations. Tech. Rep. CFDL-TR-88-1, MIT, feb.
- [21] Saxer, A. P., and Giles, M. B., 1993. "Quasi-three-dimensional nonreflecting boundary conditions for euler equations calculations". *Journal of Propulsion and Power*, **9**(2), Mar., pp. 263–271.
- [22] Hall, K. C., and Crawley, E. F., 1989. "Calculation of unsteady flows in turbomachinery using the linearized Euler equations". *AIAA Journal*, **27**(6), June, pp. 777–787.
- [23] Frey, C., and Kersken, H.-P., 2016. "ON THE REGULARISATION OF NON-REFLECTING BOUNDARY CONDITIONS NEAR ACOUSTIC RESONANCE". In Proceedings of the VII European Congress on Computational Methods in Applied Sciences and Engineering (ECCOMAS Congress 2016).
- [24] Tyler, J. M., and Sofrin, T. G., 1962. "Axial flow compressor noise studies". In SAE Technical Paper Series, SAE International.
- [25] Wang, F., Carnevale, M., Lu, G., di Mare, L., and Kulkarni, D., 2016. "Virtual gas turbine: Pre-processing and numerical simulations". In Proceedings of ASME TurboExpo, South Korea, Seoul, ASME.
- [26] Jameson, A., 1991. "Time dependent calculations using multigrid, with applications to unsteady flows past airfoils and wings". In 10th Computational Fluid Dynamics Conference, American Institute of Aeronautics and Astronautics.
- [27] van Leer, B., 1979. "Towards the ultimate conservative difference scheme. v. a second-order sequel to godunov's method". *Journal of Computational Physics*, **32**(1), July, pp. 101–136.

- [28] Wilcox, D. C., 1988. "Reassessment of the scale-determining equation for advanced turbulence models". *AIAA Journal*, **26**(11), Nov., pp. 1299–1310.
- [29] Menter, F. R., Kuntz, M., and Langtry, R., 2003. "Ten years of industrial experience with the sst turbulence model". *Turbulence, heat and mass transfer*, **4**(1), pp. 625–632.
- [30] Wang, F., Carnevale, M., di Mare, L., and Gallimore, S., 2017. "Simulation of multistage compressor at off-design conditions". *Journal of Turbomachinery*, **140**(2), Dec.
- [31] Cai, X.-C., and Sarkis, M., 1999. "A restricted additive schwarz preconditioner for general sparse linear systems". *SIAM Journal on Scientific Computing*, **21**(2), Jan., pp. 792–797.
- [32] Balay, S., Abhyankar, S., Adams, M. F., Benson, S., Brown, J., Brune, P., Buschelman, K., Constantinescu, E., Dalcin, L., Dener, A., Eijkhout, V., Gropp, W. D., Hapla, V., Isaac, T., Jolivet, P., Karpeev, D., Kaushik, D., Knepley, M. G., Kong, F., Kruger, S., May, D. A., McInnes, L. C., Mills, R. T., Mitchell, L., Munson, T., Roman, J. E., Rupp, K., Sanan, P., Sarich, J., Smith, B. F., Zampini, S., Zhang, H., Zhang, H., and Zhang, J., 2021. PETSc/TAO users manual. Tech. Rep. ANL-21/39 - Revision 3.16, Argonne National Laboratory.
- [33] Qureshi, I., Smith, A. D., Chana, K. S., and Povey, T., 2011. "Effect of temperature nonuniformity on heat transfer in an unshrouded transonic HP turbine: An experimental and computational investigation". *Journal of Turbomachinery*, **134**(1), May.
- [34] He, L., Menshikova, V., and Haller, B. R., 2004. "Influence of hot streak circumferential length-scale in transonic turbine stage". In Volume 5: Turbo Expo 2004, Parts A and B, ASMEDC.
- [35] Wang, F., and di Mare, L., 2017. "Mesh generation for turbomachinery blade passages with three-dimensional endwall features". *Journal of Propulsion and Power*, **33**(6), Nov., pp. 1459–1472.
- [36] Butler, T. L., Sharma, O. P., Joslyn, H. D., and Dring, R. P., 1989. "Redistribution of an inlet temperature distortion in an axial flow turbine stage". *Journal of Propulsion and Power*, **5**(1), Jan., pp. 64–71.
- [37] Lakshminarayana, B., and Horlock, J. H., 1973. "Generalized expressions for secondary vorticity using intrinsic co-ordinates". *Journal of Fluid Mechanics*, **59**(1), June, pp. 97–115.
- [38] Kerrebrock, J. L., and Mikolajczak, A. A., 1970. "Intra-stator transport of rotor wakes and its effect on compressor performance". *Journal of Engineering for Power*, **92**(4), Oct., pp. 359–368.
- [39] Shang, T., and Epstein, A. H., 1997. "Analysis of hot streak effects on turbine rotor heat load". *Journal of Turbomachinery*, **119**(3), July, pp. 544–553.
- [40] Smith, L. H., 1966. "Wake dispersion in turbomachines". *Journal of Basic Engineering*, **88**(3), Sept., pp. 688–690.
- [41] Zante, D. E. V., Adamczyk, J. J., Strazisar, A. J., and Okiishi, T. H., 2002. "Wake recovery performance benefit in a high-speed axial compressor". *Journal of Turbomachinery*, **124**(2), Apr., pp. 275–284.